



Supplement of

A fast surrogate model for 3D Earth glacial isostatic adjustment using Tensorflow (v2.8.0) artificial neural networks

Ryan Love et al.

Correspondence to: Ryan Love (rlove@mun.ca)

The copyright of individual parts of the supplement might differ from the article licence.

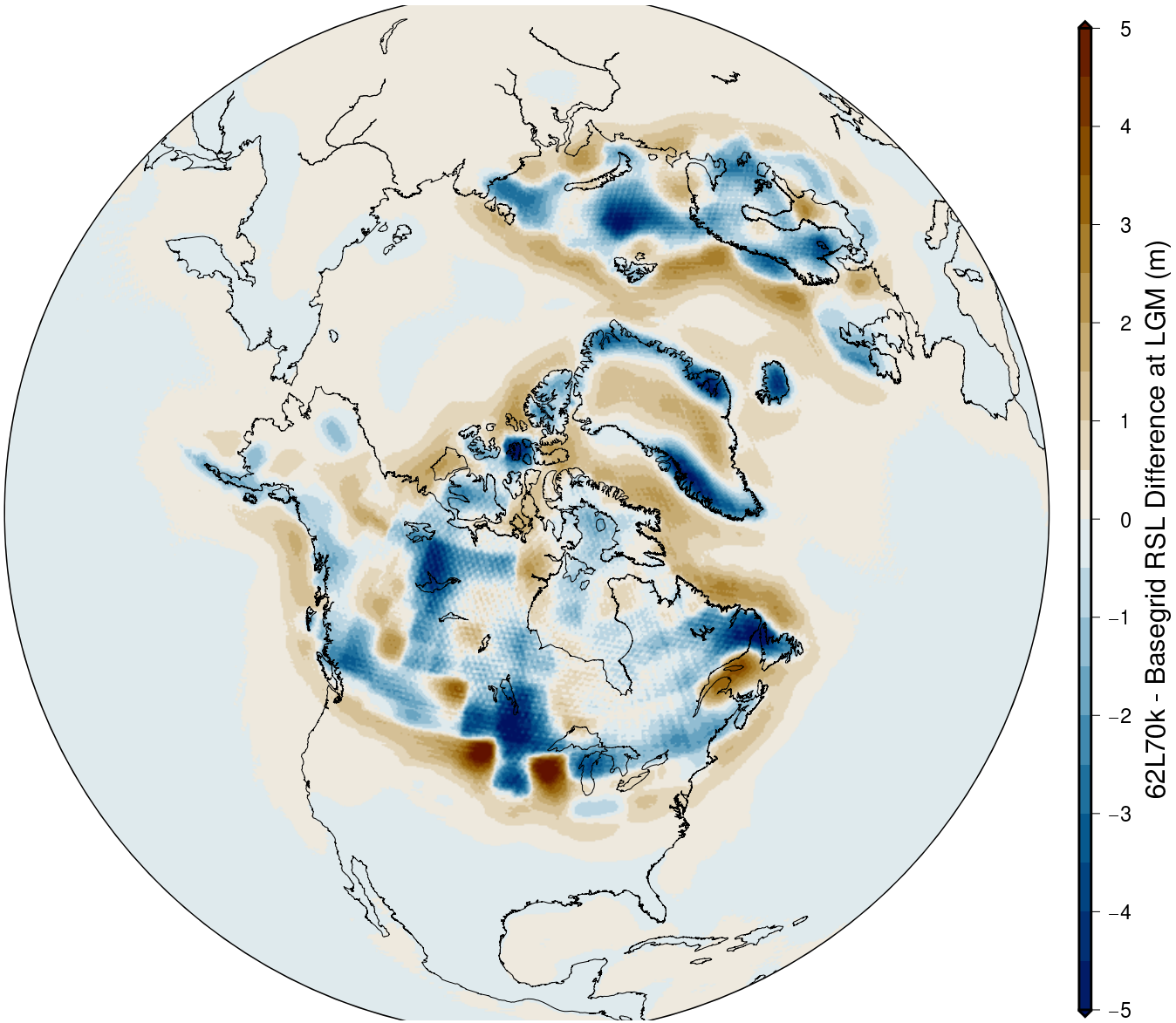


Figure S1. Difference in predicted RSL at LGM between a reduced resolution configuration (62L70k) and the more typical Seakon resolution (Basegrid). These results are for the ICE5G (Peltier, 2004) ice loading history and background radial viscosity profile of a 120km thick elastic lithosphere, $3 \times 10^{21} \text{ Pa} \cdot \text{s}$ upper mantle viscosity, and $90 \times 10^{21} \text{ Pa} \cdot \text{s}$ lower mantle viscosity. This SS profile was chosen as it performed well for the USEC database in previous investigations (Love et al., 2016). The Seakon model results shown here are comparisons between spherically symmetric configurations. Tests involving lateral variability structure give comparable results.

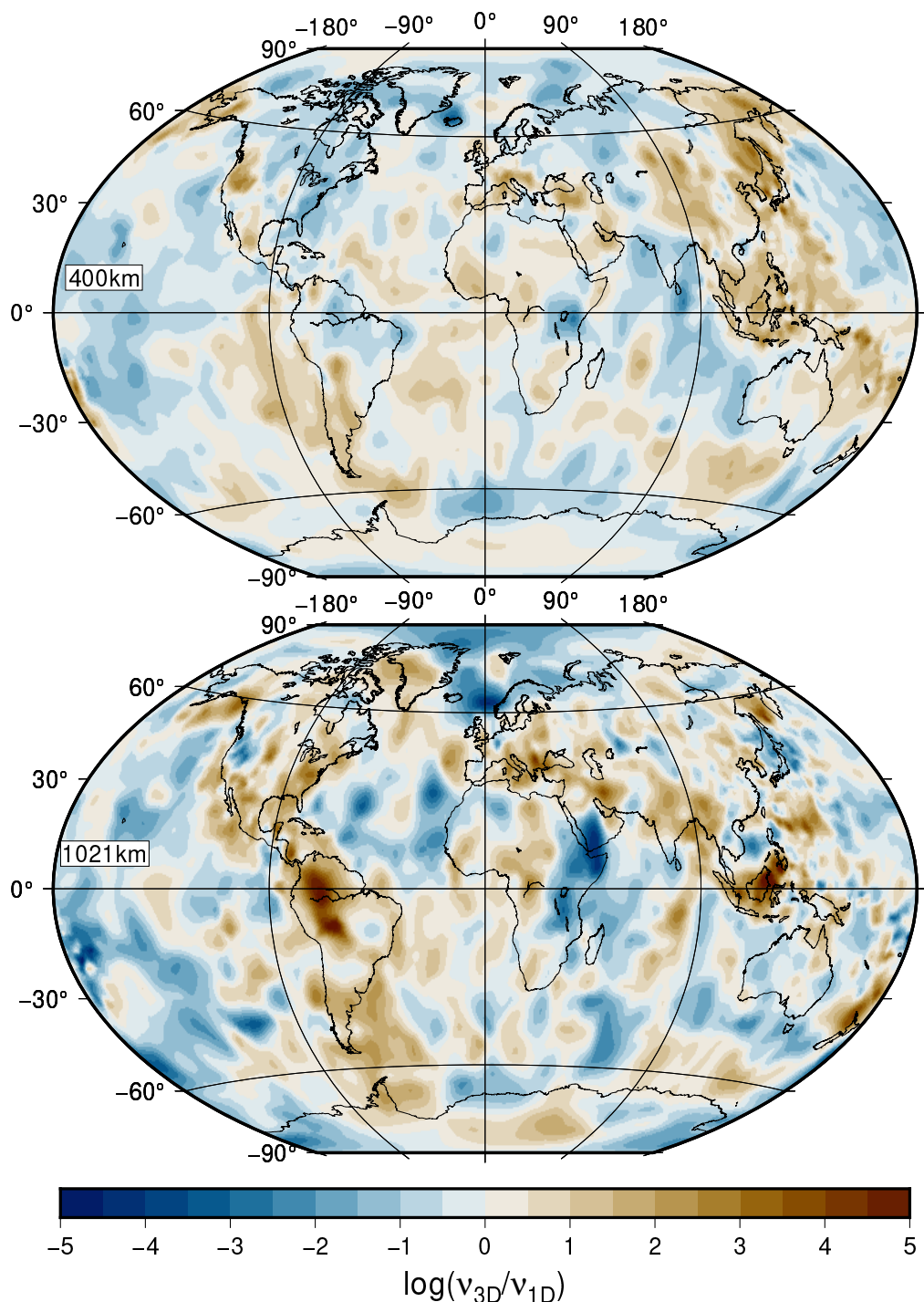


Figure S2. Panels show spatial viscosity variations as $\log(\nu_{3D}/\nu_{SS})$ for two depths in the mantle, 400 km and 1021 km, derived from the Savani shear wave velocity model. A value of zero indicates that the viscosity value at that location is equivalent to the background spherically symmetric Earth model.

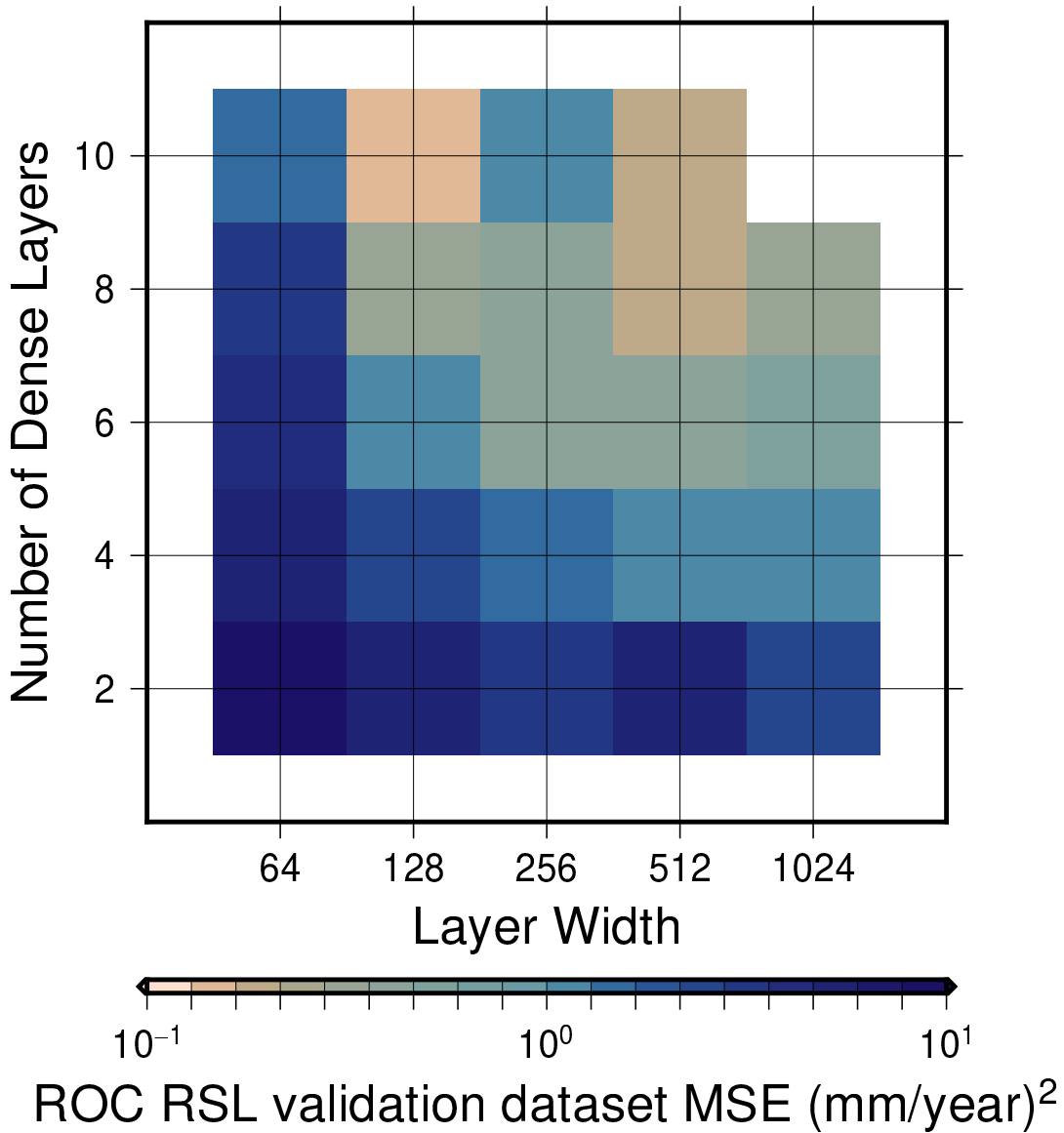


Figure S3. Preliminary results showing the mean square error from the validation set calculated during model training for a range of neural network architectures. As with the network described in the main text, each dense layer is paired with a normalization layer. Unlike the network described in the main text, each layer has the same width. The input dataset used during this initial set of tests was a subset of the semi-3D S40RTS configuration with only the 71km thick lithosphere. Filtering of the input dataset was also conducted differently by comparison to the main investigation. The input was filtered based on the presence of ice during the previous 4 timesteps, with greater weights placed on data which had nonzero values for ice thickness.

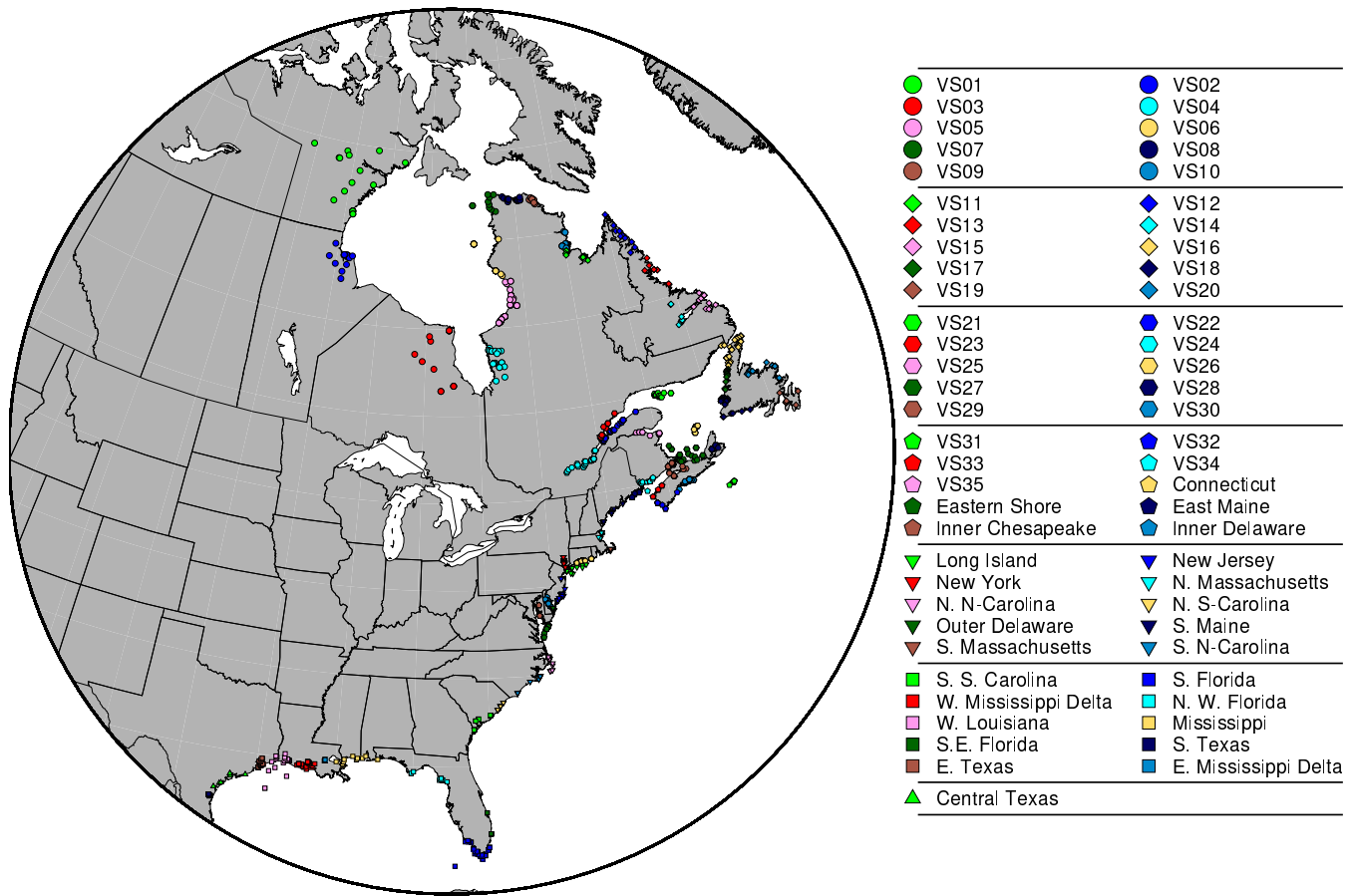


Figure S4. Locations of sea-level index points, terrestrial limiting, marine limiting data are shown as coloured symbols. The shape and colour reflect the groupings of each data-point. VS01 through VS35 are sites 1 through 35 from Vacchi et al. (2018). Connecticut through to S. South-Carolina are from Engelhart and Horton (2012). S.E. Florida to S. Texas are from Love et al. (2016).

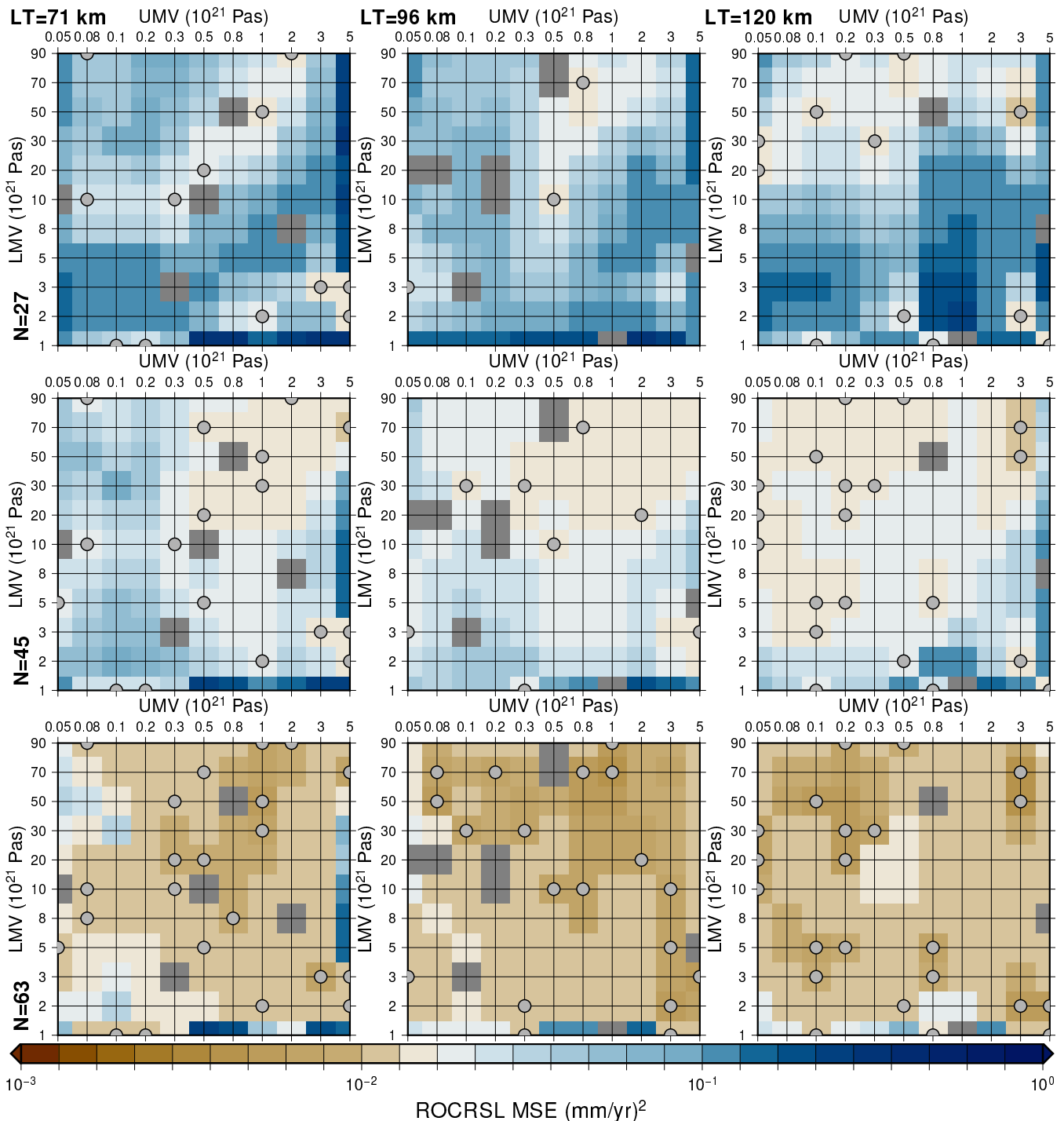


Figure S5. Plot shows the MSE (for all locations and time-steps) through parameter space (LT/UMV/LMV) for input training datasets with $N=27$ (top row), 45 (middle row), and 63 (bottom row) for the Savani+LR18 ROC RSL ANN. Parameter vectors included in training dataset are indicated by grey circles. Columns give results for the three values of global-mean elastic lithosphere thickness: 71 km (left), 96 km (middle), 120 km (right). Note that results which are anomalous and were affected by technical issues for specific ensemble members are rendered here in grey.

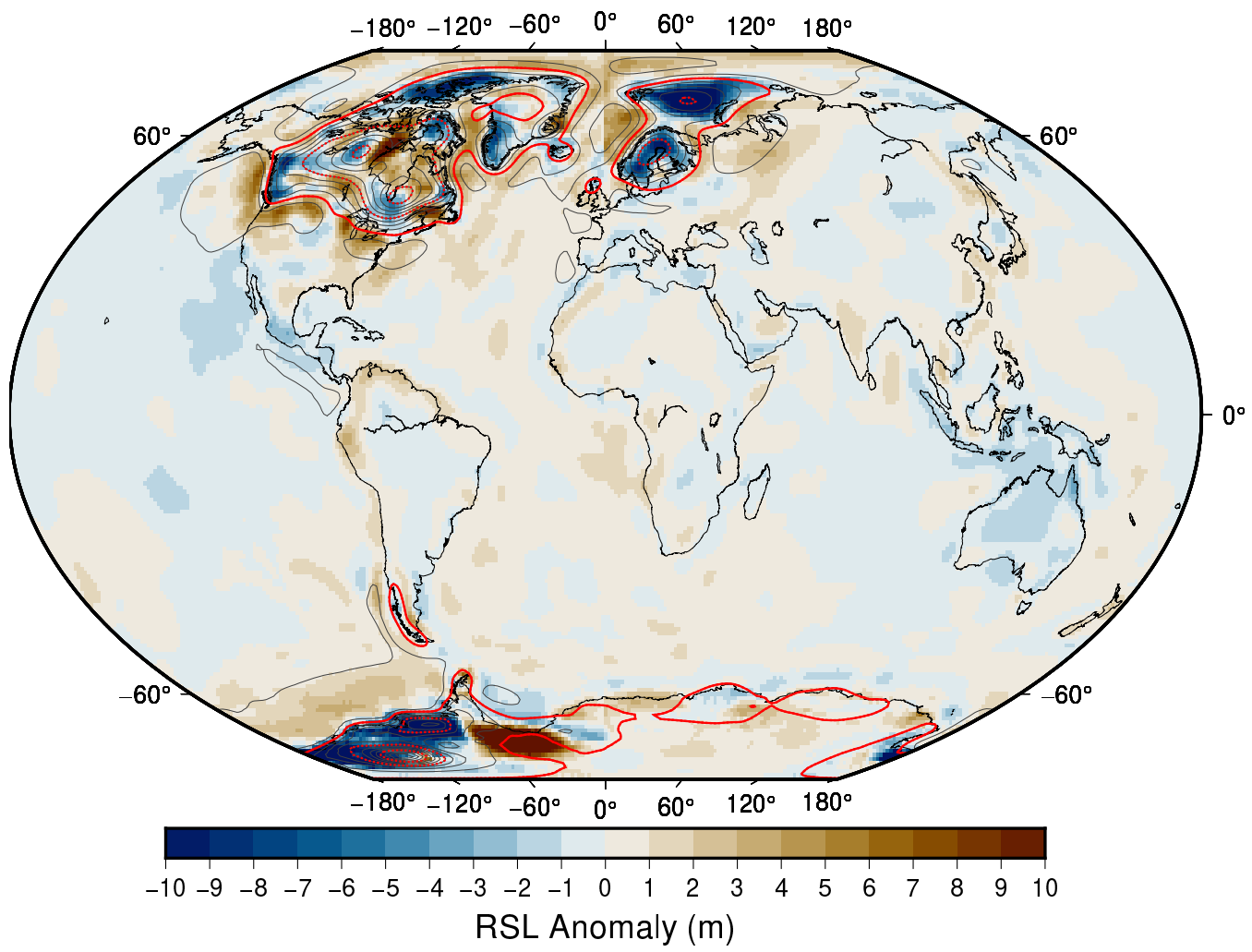


Figure S6. RSL anomaly, emulated RSL field minus explicit (3D-SS Seakon + NMSS) RSL field for the S40RTS+LR18 case, at 10 ka. Grey contours denote the RSL field (from Seakon) in 25 m increments, dotted red contours denote 100 m increments, and the solid red contour denotes RSL values of 0 m. The parameter vector plotted is that with the median MSE, calculated for all spatio-temporal data, for the $N = 45$ results.

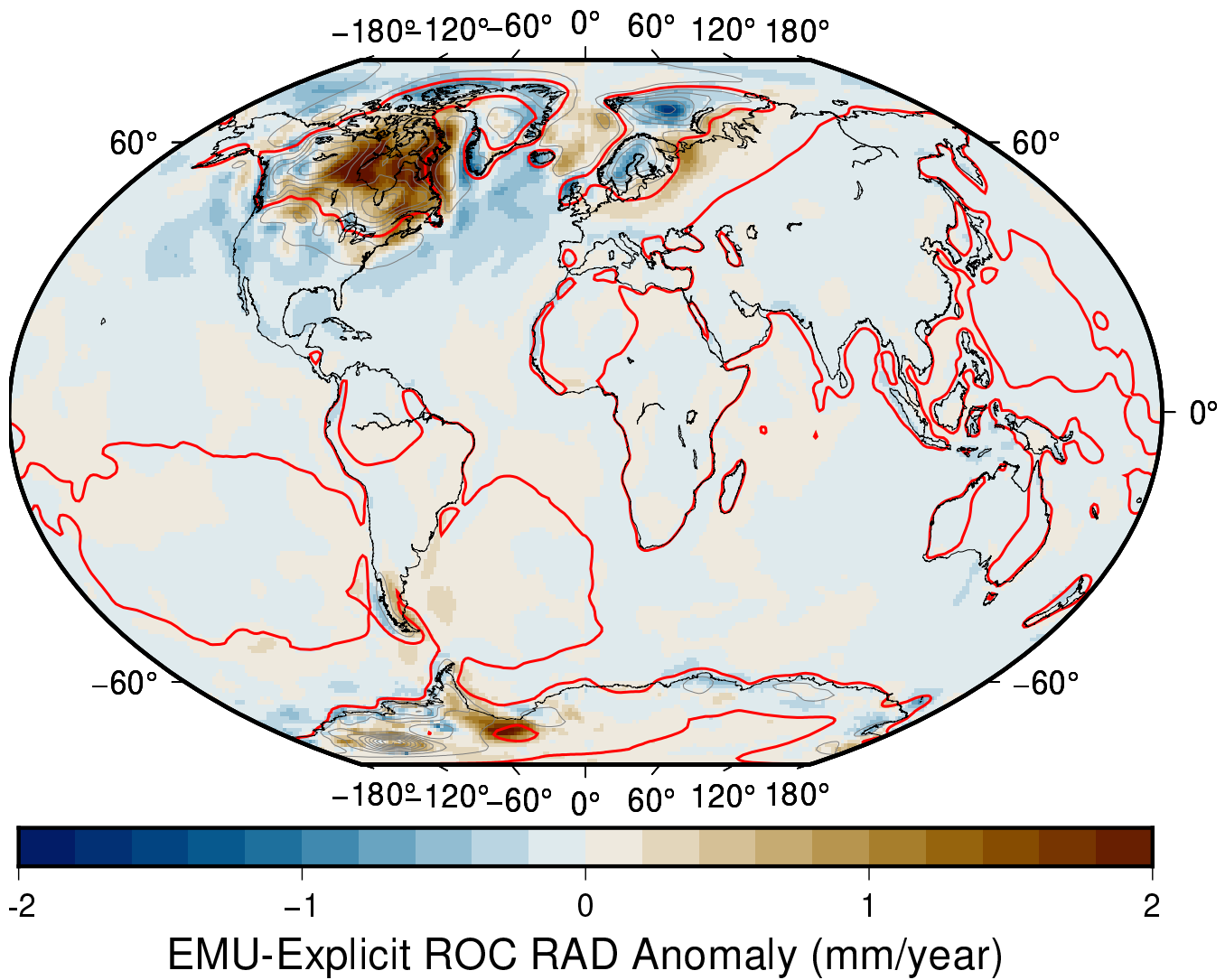


Figure S7. ROC RAD anomaly, emulated field minus 3D-SS field added to the NMSS output for the S40RTS+LR18 case, at present day. Contours denote the ROC RAD field (from 3D-SS+NMSS) in 2 mm/yr increments, the red line denotes the 0 mm/yr contour. The parameter vector plotted is that with the median MSE, calculated for all spatio-temporal data, for the $N = 45$ ANN.

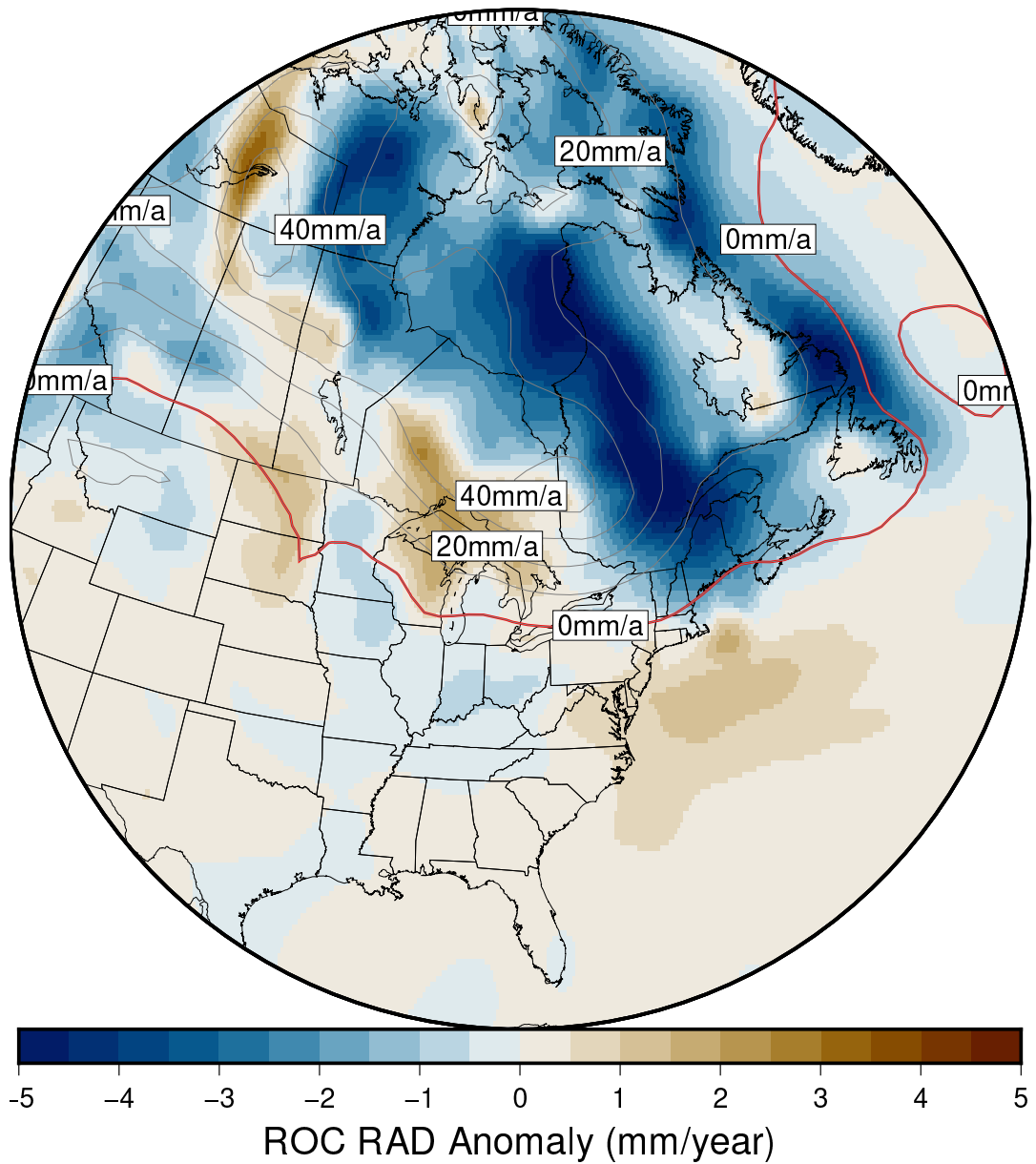


Figure S8. ROC RAD anomaly, emulated field minus 3D-SS field added to the NMSS output for the S40RTS+LR18 case, at 10ka. Contours denote the ROC RAD field (from from 3D-SS+NMSS) in 10 mm/yr increments, the red line denotes the 0 mm/yr contour. The parameter vector plotted is that with the median MSE, calculated for all spatio-temporal data, for the N = 45 ANN.

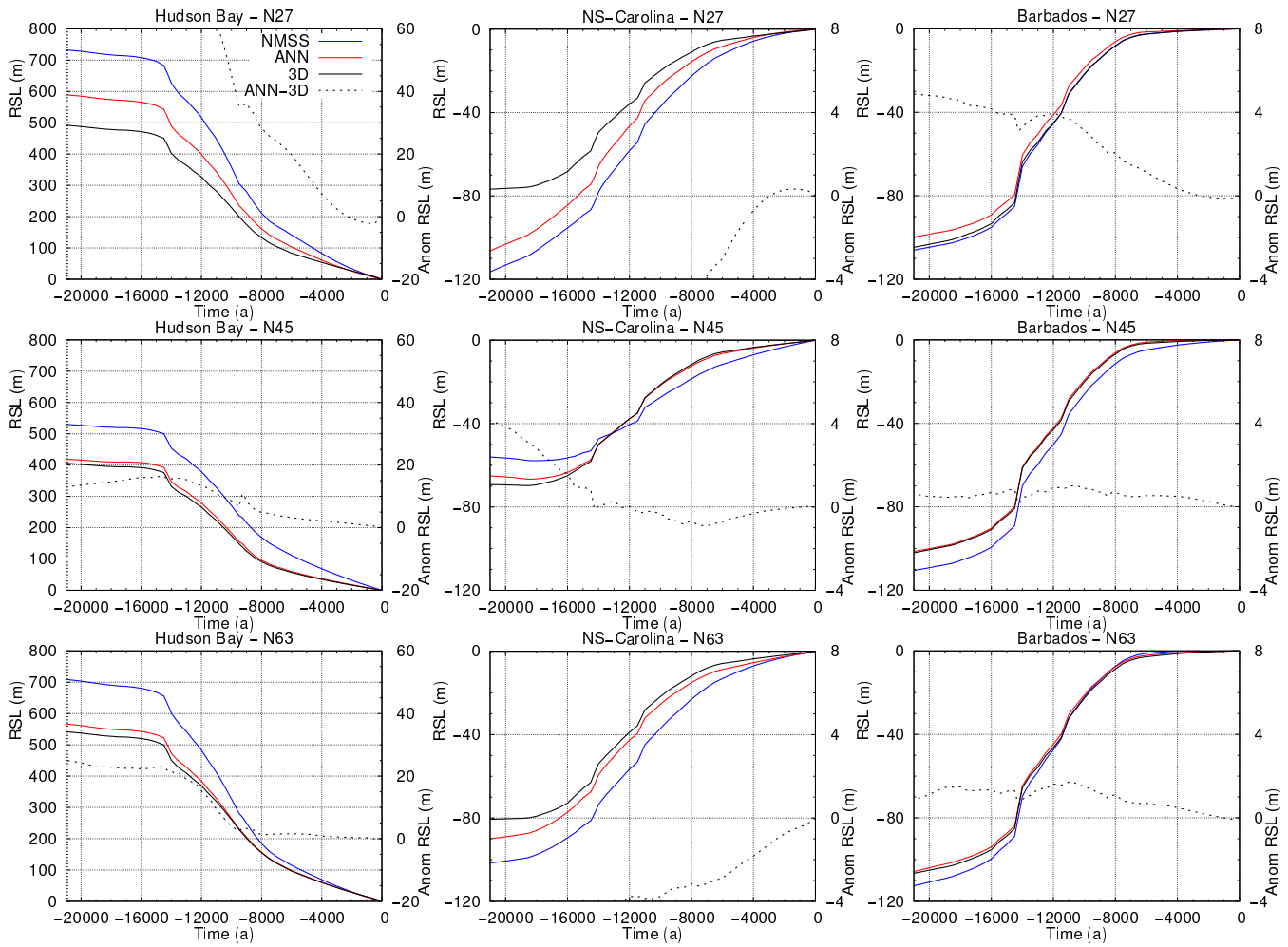


Figure S9. RSL timeseries for near- (Hudson Bay), intermediate- (Northern S-Carolina), and far-field (Barbados) locations, for the N=27, 45 and 63 ANN training sets. RSL curves are computed using the parameter vector corresponding to the median MSE for each validation ensemble. As the parameter vector for the mean MSE generally varies with N, the resulting RSL curves also change. 3D Earth model configuration shown is S40RTS with a SS lithosphere.

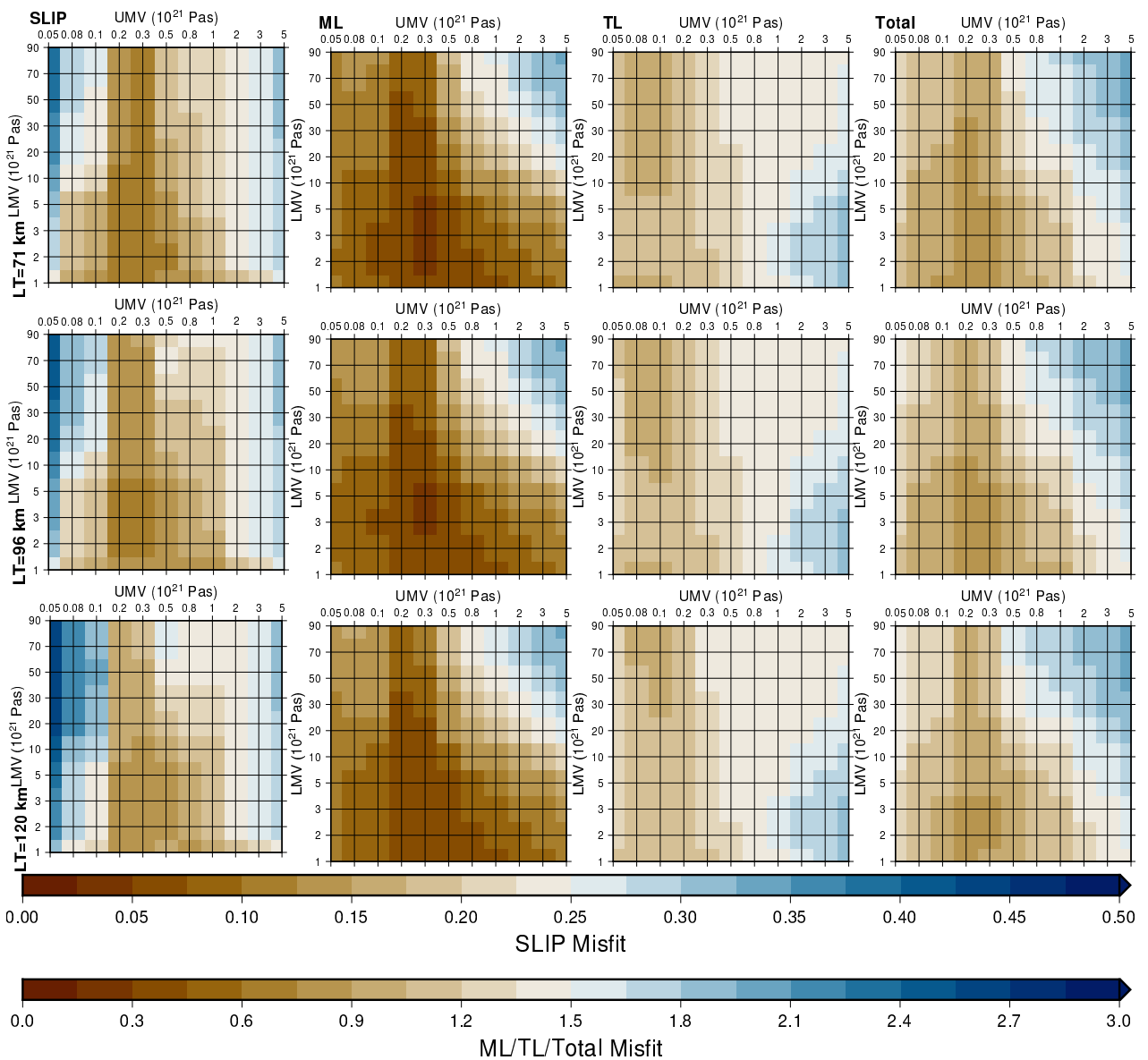


Figure S10. Proxy-data:model misfit for RSL database through parameter space (LT/UMV/LMV) for explicit 3D model output (NMSS plus 3D-SS from Seakon) for S40RTS+LR18. Columns from left to right show marine limiting, SLIP, terrestrial limiting, and total misfits respectively, while rows are 71, 96, and 120 km respectively. Misfit plotted is calculated as in equations 1 and 2.

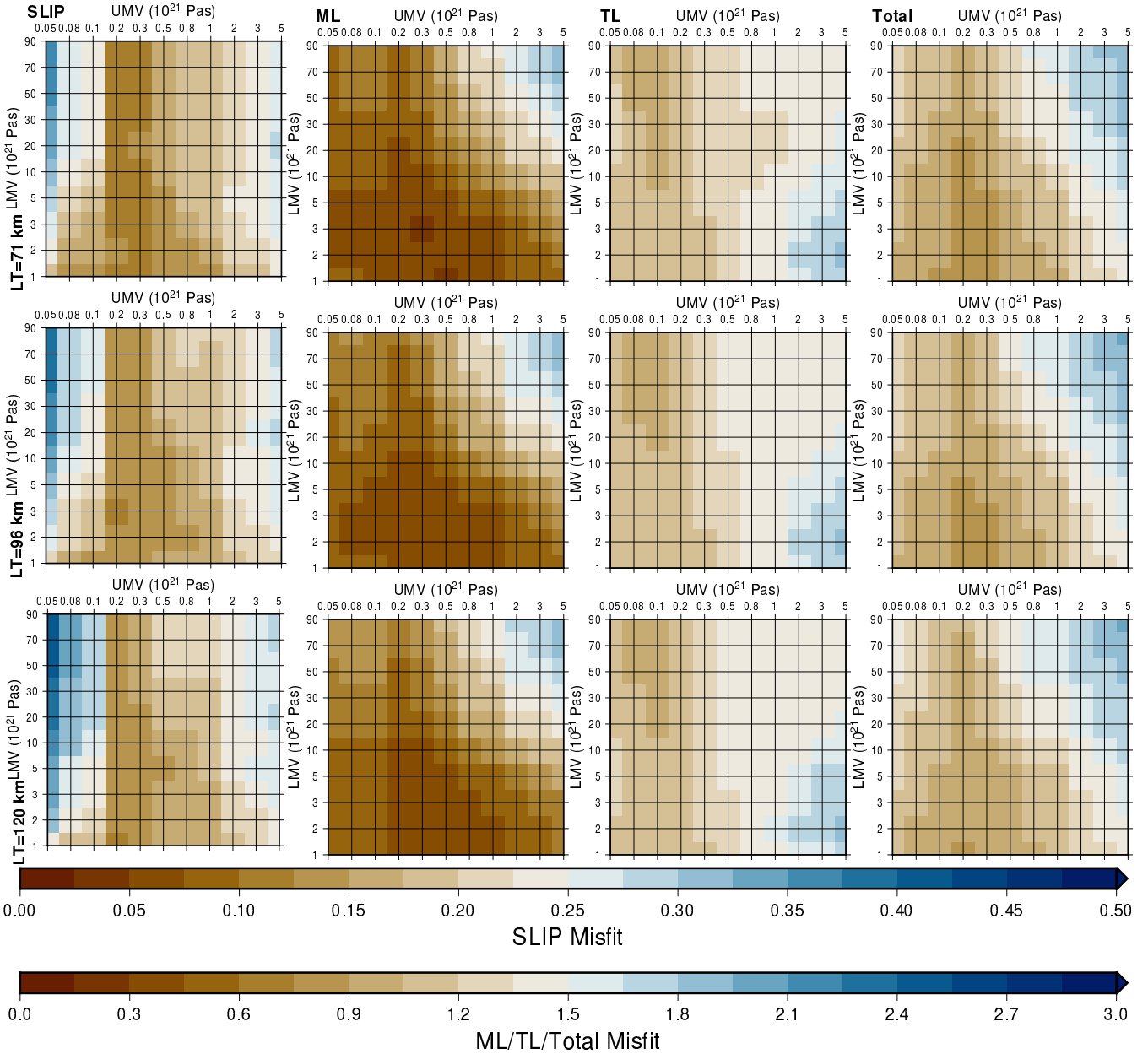


Figure S11. Proxy-data:model misfit for RSL database through parameter space (LT/UMV/LMV) for the NMSS model modified with the ANN to emulate S40RTS with the LR18 lithosphere model 3D Earth model. Columns from left to right show marine limiting, SLIP, terrestrial limiting, and total misfits respectively, while rows are 71, 96, and 120 km respectively. Misfit plotted is calculated as in equations 1 and 2.

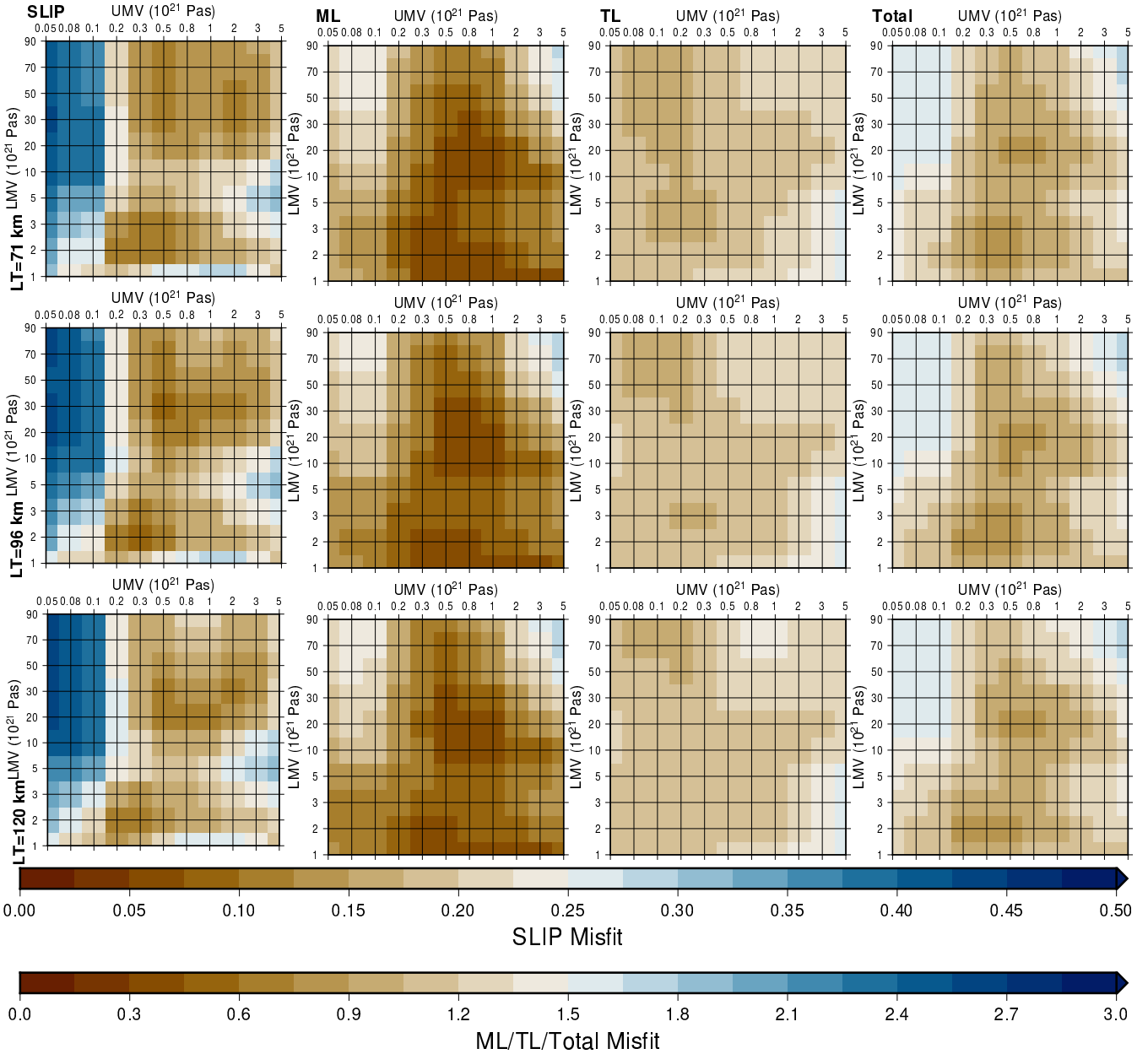


Figure S12. Proxy-data:model misfit for RSL database through parameter space (LT/UMV/LMV) for the NMSS model. Columns from left to right show marine limiting, SLIP, terrestrial limiting, and total misfits respectively, while rows are 71, 96, and 120 km respectively. Misfit plotted is calculated as in equations 1 and 2.

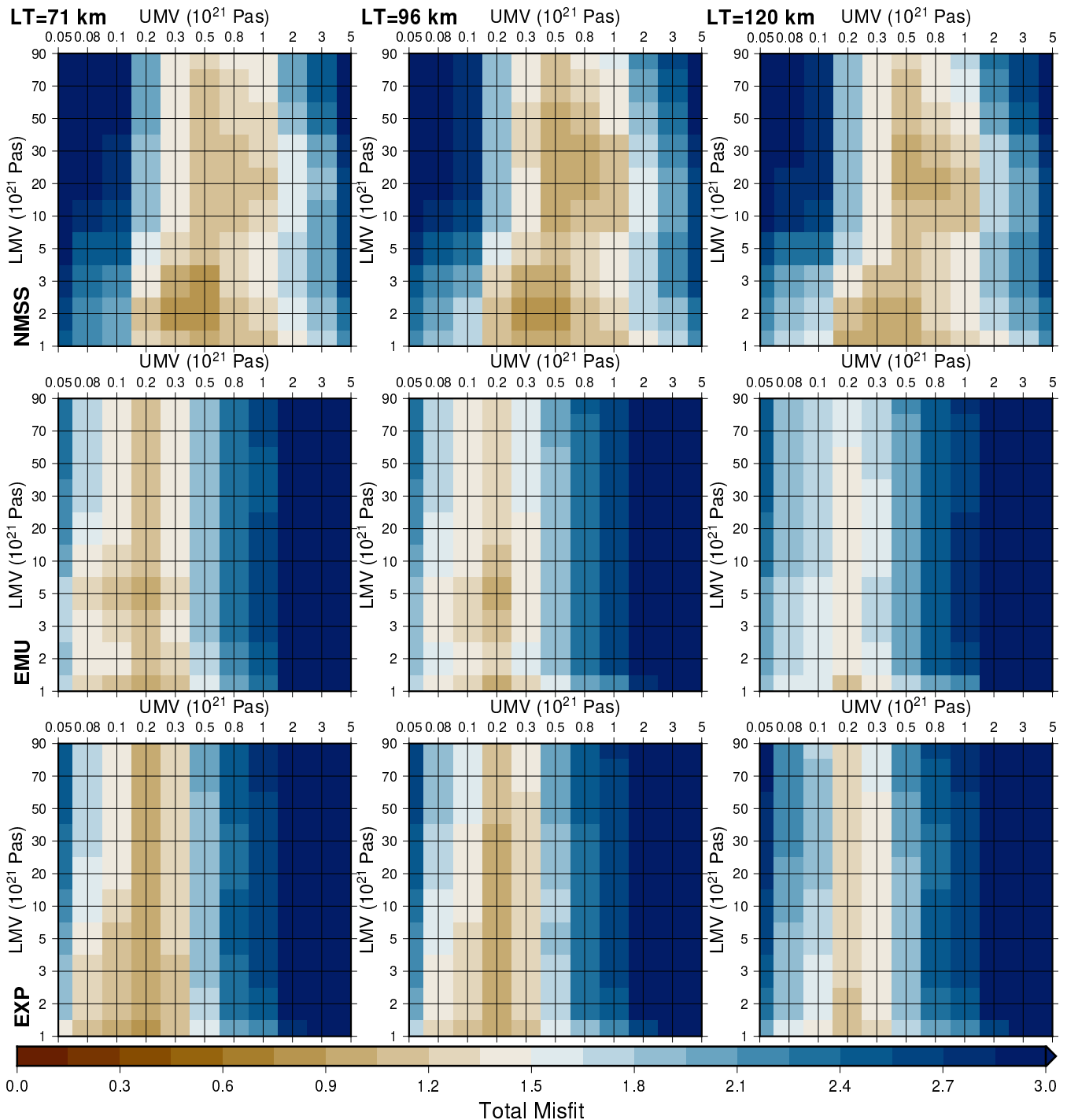


Figure S13. Model: data misfit across the CAAC RSL database through parameter space (LT/UMV/LMV). Top row is NMSS model output, middle row is emulated 3D model output (NMSS plus emulated 3D-SS from Seakon), bottom row is explicit (NMSS plus 3D-SS from Seakon) output. Misfit plotted is calculated as in equations 1 and 2 and total misfit has been plotted.

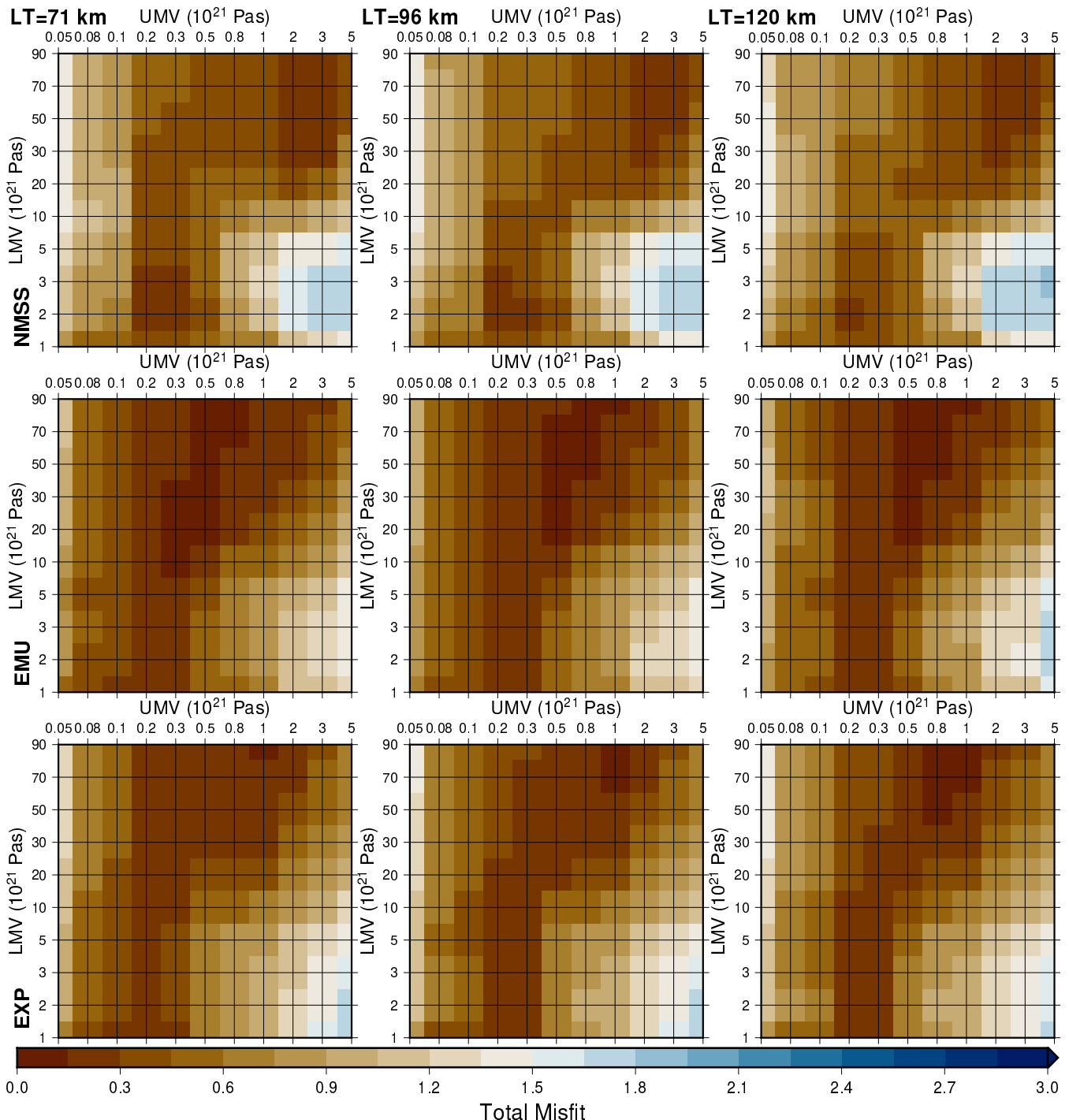


Figure S14. Model: data misfit across the USEC RSL database through parameter space (LT/UMV/LMV). Top row is NMSS model output, middle row is emulated 3D model output (NMSS plus emulated 3D-SS from Seakon), bottom row is explicit (NMSS plus 3D-SS from Seakon) output. Misfit plotted is calculated as in equations 1 and 2 and total misfit has been plotted.

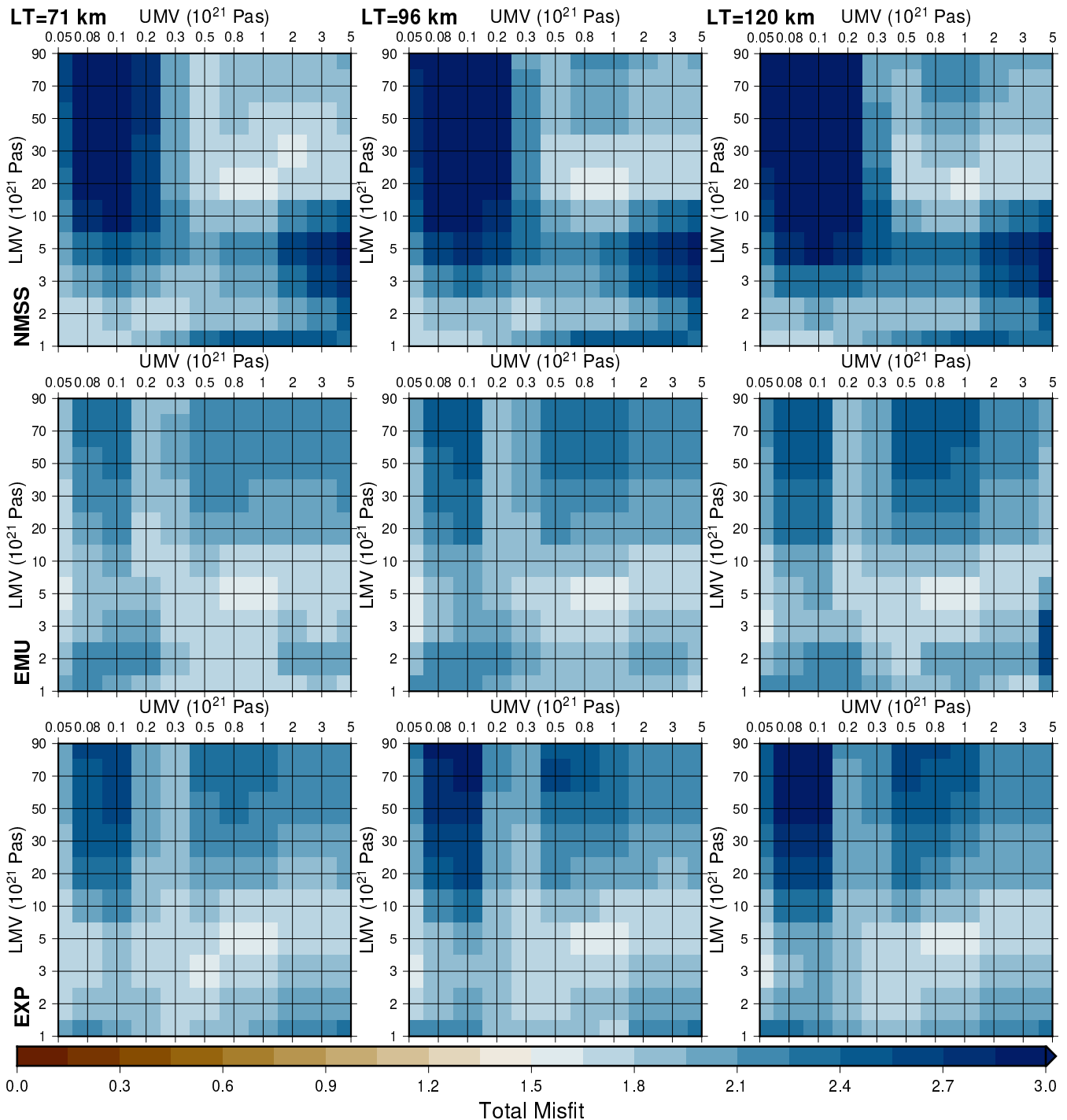


Figure S15. Model: data misfit across the USGC RSL database through parameter space (LT/UMV/LMV). Top row is NMSS model output, middle row is emulated 3D model output (NMSS plus emulated 3D-SS from Seakon), bottom row is explicit (NMSS plus 3D-SS from Seakon) output. Misfit plotted is calculated as in equations 1 and 2 and total misfit has been plotted.

References

- Engelhart, S. E. and Horton, B. P.: Holocene sea level database for the Atlantic coast of the United States, *Quaternary Science Reviews*, 54, 12–25, <https://doi.org/10.1016/j.quascirev.2011.09.013>, 2012.
- 5 Love, R., Milne, G. A., Tarasov, L., Engelhart, S. E., Hijma, M. P., Latychev, K., Horton, B. P., and Törnqvist, T. E.: The contribution of glacial isostatic adjustment to projections of sea-level change along the Atlantic and Gulf coasts of North America, *Earth's Future*, 4, 440–464, <https://doi.org/10.1002/2016ef000363>, 2016.
- Peltier, W.: Global Glacial Isostasy and the Surface of the Ice-Age Earth: The ICE-5G (VM2) Model and GRACE, *Annual Review of Earth and Planetary Sciences*, 32, 111–149, <https://doi.org/10.1146/annurev.earth.32.082503.144359>, 2004.
- 10 Vacchi, M., Engelhart, S. E., Nikitina, D., et al.: Postglacial relative sea-level histories along the eastern Canadian coastline, *QSR*, 201, 124–146, <https://doi.org/10.1016/j.quascirev.2018.09.043>, 2018.